



**HAL**  
open science

## Aqueous-phase oligomerization of methyl vinyl ketone through photooxidation - Part 1: Aging processes of oligomers

P. Renard, F. Siekmann, G. Salque, C. Demelas, Bruno Coulomb, Laurent Vassalo, S. Ravier, B. Temime-Roussel, D. Voisin, Anne Monod

► **To cite this version:**

P. Renard, F. Siekmann, G. Salque, C. Demelas, Bruno Coulomb, et al.. Aqueous-phase oligomerization of methyl vinyl ketone through photooxidation - Part 1: Aging processes of oligomers. *Atmospheric Chemistry and Physics*, 2015, 15 (1), pp.21-35. 10.5194/acp-15-21-2015 . hal-01436863

**HAL Id: hal-01436863**

**<https://hal.science/hal-01436863>**

Submitted on 25 Jun 2018

**HAL** is a multi-disciplinary open access archive for the deposit and dissemination of scientific research documents, whether they are published or not. The documents may come from teaching and research institutions in France or abroad, or from public or private research centers.

L'archive ouverte pluridisciplinaire **HAL**, est destinée au dépôt et à la diffusion de documents scientifiques de niveau recherche, publiés ou non, émanant des établissements d'enseignement et de recherche français ou étrangers, des laboratoires publics ou privés.



Distributed under a Creative Commons Attribution 4.0 International License



# Aqueous-phase oligomerization of methyl vinyl ketone through photooxidation – Part 1: Aging processes of oligomers

P. Renard<sup>1</sup>, F. Siekmann<sup>1</sup>, G. Salque<sup>2</sup>, C. Demelas<sup>1</sup>, B. Coulomb<sup>1</sup>, L. Vassalo<sup>1</sup>, S. Ravier<sup>1</sup>, B. Temime-Roussel<sup>1</sup>, D. Voisin<sup>2</sup>, and A. Monod<sup>1</sup>

<sup>1</sup>Aix-Marseille Université, CNRS, LCE FRE 3416, 13331, Marseille, France

<sup>2</sup>Université Joseph Fourier, Grenoble 1/CNRS-INSU, Laboratoire de Glaciologie et Géophysique de l'Environnement, 54 rue Molière, 38402 Saint-Martin-d'Hères, France

Correspondence to: P. Renard (pascal.renard@etu.univ-amu.fr)

Received: 11 April 2014 – Published in Atmos. Chem. Phys. Discuss.: 12 June 2014

Revised: 24 November 2014 – Accepted: 1 December 2014 – Published: 7 January 2015

**Abstract.** It has recently been established that unsaturated water-soluble organic compounds (UWSOCs) might efficiently form oligomers in polluted fogs and wet aerosol particles, even for weakly soluble ones like methyl vinyl ketone (MVK). The atmospheric relevance of these processes is explored by means of multiphase process model studies in a companion paper. In the present study, we investigate the aging of these aqueous-phase MVK oligomers formed via  $\bullet\text{OH}$  oxidation, as well as their ability to form secondary organic aerosol (SOA) upon water evaporation. The comparison between aqueous-phase composition and aerosol composition after nebulization of the corresponding solutions shows similar trends for oligomer formation and aging. The measurements reveal that oligomer aging leads to the formation of organic diacids. Quantification of the SOA mass formed after nebulization is performed, and the obtained SOA mass yields seem to depend on the spectral irradiance of the light used to initiate the photochemistry. Investigating a large range of initial MVK concentrations (0.2–20 mM), the results show that their  $\bullet\text{OH}$  oxidation undergoes competition between functionalization and oligomerization that is dependent on the precursor concentration. At high initial MVK concentrations ( $\geq 2$  mM), oligomerization prevails over functionalization, while at lower initial concentrations, oligomerization is not the major process, and functionalization dominates, resulting in small carbonyls, dicarbonyls and monoacids. The atmospheric implications of these processes are discussed.

## 1 Introduction

Organic aerosol plays an important role in many atmospheric processes and has an important impact on climate and human health. Globally, about 20% of the organic aerosol mass is emitted directly (Kanakidou et al., 2005; Spracklen et al., 2011), which conversely indicates the relevance of aerosol formed by transformation of organic gas-phase species, i.e. secondary organic aerosol (SOA). The most commonly studied mechanism of SOA formation is the oxidation of volatile organic compounds (VOCs), which can lead to the formation of less volatile species that subsequently partition into the condensed phase (Donahue et al., 2011; Kanakidou et al., 2005; Kroll and Seinfeld, 2008; Hallquist et al., 2009). Nevertheless, the oxidation of VOCs also results in more water-soluble products that readily partition into the aqueous phase (Blando and Turpin, 2000; Ervens et al., 2011; Epstein et al., 2013). Due to further reactivity in the liquid phase, higher molecular weight and less volatile compounds can be formed, which can remain at least in part in the condensed phase upon water evaporation, thus leading to additional secondary organic aerosol formation through aqueous-phase reactions (aqSOA) (El Haddad et al., 2009; Carlton et al., 2009; Ervens et al., 2011; Ortiz-Montalvo et al., 2012). In particular, Lee et al. (2012) observed a significant enhancement of organic mass during the initial stage of oxidation of cloud water organics, which they explained by functionalizing dissolved volatile organics via hydroxyl radical ( $\bullet\text{OH}$ ) oxidation. Aqueous-phase processes can be very different from those in the gas phase, thus leading to aqSOA

with likely very different physical and chemical properties (Ervens et al., 2011; Ortiz-Montalvo et al., 2012). These differences can explain that the oxidation state of SOA formed during dry smog chamber experiments is significantly lower than that of ambient SOA (Kroll and Seinfeld, 2008; Aiken et al., 2008; De Carlo et al., 2008; Ng et al., 2010; Lee et al., 2012).

Volkamer et al. (2007) suggested that chemical processes in the aqueous phase of hygroscopic particles, such as wet aerosol, can efficiently contribute to aqSOA mass. Besides, wet aerosol provides higher precursor concentrations than in cloud and fog water droplets and reside in the atmosphere over hours or days (Ervens et al., 2011), suggesting a significant role for aqSOA formation in wet aerosol, in particular, in regions with high relative humidity (Carlton and Turpin, 2013) and hygroscopic aerosol. Isoprene has the largest global atmospheric emissions, estimated at  $\sim 600 \text{ Tg yr}^{-1}$  of all non-methane VOCs (Guenther et al., 2006). Its key oxidation products – i.e. methacrolein (MACR) and hydroperoxides (Kroll et al., 2006) – are known to contribute directly to the formation of SOA in the atmosphere. Methyl vinyl ketone (MVK) is the other main gas-phase oxidation product of isoprene, yielding from 32 to 44 % (Lee et al., 2005, Kroll et al., 2006). Unlike MACR, MVK does not lead to the formation of SOA during its gas-phase photooxidation (Kroll et al., 2006; Surratt et al., 2006), likely because of the lack of an aldehydic hydrogen which precludes the formation of acidic products such as 2,3-dihydroxymethacrylic acid (2-MGA) for further particle-phase esterification reactions (Surratt et al., 2006). However, these results were obtained in smog chamber experiments performed under dry conditions where aqueous-phase processes were excluded.

The photooxidation of carbonyl compounds has been studied in the aqueous phase, and their ability to form oligomers and potentially aqSOA was shown (Altieri et al., 2006 and 2008; Carlton et al., 2006 and 2007; Perri et al., 2009; El Haddad et al., 2009; Tan et al., 2009, 2010 and 2012; Zhang et al., 2010; Zhao et al., 2012; Liu et al., 2012; Ortiz-Montalvo et al., 2012; Lim et al., 2013; Renard et al., 2013; Kameel et al., 2013; Kameel et al., 2014; Daumit et al., 2014). In particular, Renard et al. (2013) showed that  $\bullet\text{OH}$  oxidation of MVK in the aqueous phase proceeds via a radical mechanism leading to oligomers which molecular masses up to 1800 Da, with the precursor initial concentration from 2 to 20 mM. At lower precursor initial concentrations (e.g. 0.2 mM of MVK), Renard et al. (2013) observed lower-weight molecular compounds (up to  $m/z$  300), and Zhang et al. (2010) observed the formation of small oxidized compounds, such as methylglyoxal, formaldehyde, acetic, formic and pyruvic acids – thus suggesting a competition between functionalization and oligomerization at these low initial concentrations.

Liu et al. (2012) showed the ability of the generated oligomers to form SOA after water evaporation. It is thus likely that the atmospheric impact of MVK reactivity, and

**Table 1.** Experimental conditions of  $\bullet\text{OH}$  oxidation of MVK in the aqueous phase. All experiments are performed at 25 °C. Time 0 corresponds to MVK injection in the photoreactor (samples taken at 0, 5, 10, 15, 30, 50, 75, 105, 150 min). Aqueous-phase characterization was performed using UPLC-ESI-MS and UHPLC-UV for all experiments, and IC-ESI-MS analyses were made only during experiments A and B. Aerosol characterization after nebulization using SMPS and AMS was performed for all experiments.

Exp. name	[MVK] <sub>0</sub> (mM)	[H <sub>2</sub> O <sub>2</sub> ] <sub>0</sub> (mM)	MVK 90 % Consumption time (min)
A	20	400	120
B	5	100	50
C	2	40	30
D	0.5	10	25
E	0.2	4	20

especially its ability to form SOA, is very different under dry and humid conditions.

The aim of the present study is to investigate the aging of the oligomers formed through aqueous-phase photooxidation of MVK. We determine the SOA chemical composition during the formation and aging of the aqueous-phase oligomers, and we revisit the corresponding SOA mass yields. A large range of initial precursor concentrations (from 0.2 to 20 mM) is investigated in order to study the competition between functionalization and oligomerization.

## 2 Experimental

A photoreactor was used to simulate the aqueous-phase photooxidation of MVK.  $\bullet\text{OH}$  radicals were generated from H<sub>2</sub>O<sub>2</sub> photolysis (Table 1). The liquid phase was analysed using a variety of analyzers for qualitative and quantitative characterization of the solution (detailed in Sect. 2.2).

For aerosol generation, aliquots of the solution were sampled from the photoreactor at specific reaction times, then nebulized and dried prior to aerosol characterization using a scanning mobility particle sizer (SMPS) and a high-resolution time-of-flight aerosol mass spectrometer (HR-ToF-AMS) (Fig. 1). Each experiment, i.e. aqueous-phase photooxidation and aerosol generation, was repeated at least once.

### 2.1 Photoreactor

The photoreactor set-up was based on the one described by Renard et al. (2013). It was a 450 cm<sup>3</sup> Pyrex thermostated photoreactor, equipped with a 1000 W Xenon arc lamp (LOT-Oriel, LSH 601) and a glass filter (ASTM 490 AM 0). The resulting spectral irradiance into the reactor is compared to that of the sun at sea level for a 48.3° zenith angle in Fig. S1 (Supplement 2, Fig. S1). All experiments were performed at 25 °C

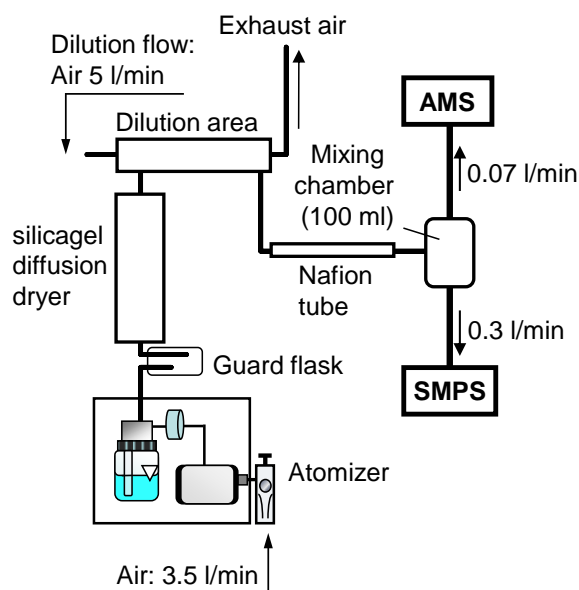


**Figure 1.** Schematic overview of the aerosol generation set-up.

and started with irradiation of UHQ water (18.2 M $\Omega$  cm, Millipore). Then H<sub>2</sub>O<sub>2</sub> (Acros, 30 %, non-stabilized) was introduced, and after 10 min of H<sub>2</sub>O<sub>2</sub> photolysis, MVK (Sigma Aldrich, 99 %) was introduced at time 0.

Tan et al. (2010) and Renard et al. (2013) have shown the important impact of initial concentrations on oligomer formation. The experiments were thus carried out with various MVK initial concentrations (Table 1), i.e. 0.2, 0.5, 2, 5 and 20 mM, corresponding to 9.6 to 960 mg CL<sup>-1</sup>. Considering MVK as a proxy for unsaturated water-soluble organic compounds (UWSOCs), this concentration range is comprised in the range of the estimated total UWSOC concentrations from fog droplets to wet aerosol (Renard et al., 2013).

The 50 cm<sup>3</sup> gas-phase head space of the photoreactor was opened to ambient air for a few seconds during each sampling. We verified in control experiments that this procedure induced insignificant losses of MVK from the solution. Since the photoreactor was closed most of the time, this procedure also induced a decrease in the dissolved O<sub>2</sub> concentrations, at a rate that was dependent on the initial reactant concentrations, as shown in the companion paper by Ervens et al. (2011).

The initial H<sub>2</sub>O<sub>2</sub> concentrations were chosen in order to obtain a ratio ( $\frac{[H_2O_2]_0}{[MVK]_0} = 20$ ), in order to favour  $\bullet$ OH reaction with MVK rather than with H<sub>2</sub>O<sub>2</sub> by more than 90 %. Under these conditions,  $\bullet$ OH concentrations were estimated in the range (2–6)  $\times 10^{-14}$  M (see Supplement 3), which falls in the range of the estimated values for  $\bullet$ OH concentrations in cloud and fog droplets (Herrmann et al., 2010; Ervens and Volkamer, 2010 and Arakaki et al., 2013).

## 2.2 Aqueous-phase characterization

Aliquots of the solution sampled from the photoreactor were analysed for qualitative structure elucidation of the oligomers using ultra-performance liquid chromatography mass spectrometry (UPLC-ESI-MS); and for quantitative studies of the concentrations of (i) MVK and H<sub>2</sub>O<sub>2</sub> by liquid chromatography coupled to UV detection (UHPLC-UV), (ii) carboxylic acids by ion chromatography–mass spectrometry (IC-ESI-MS), and (iii) oligomers using preparative liquid chromatography associated with total organic carbon (TOC) analyses.

### 2.2.1 UPLC-ESI-MS analyses

Aliquots of the solution sampled from the photoreactor were analysed for organic species using an ultra-high-performance liquid chromatographic system coupled to a time-of-flight mass spectrometer equipped with an electrospray source and an ion mobility cell (Synapt-G2 HDMS, Waters). The mass spectrometer was tuned to V-mode with a resolving power of 18 000 at  $m/z$  400. The mass accuracy (< 5 ppm) allowed for the determination of elemental composition of organic species (Renard et al., 2013 and 2014), using the I-FIT software. The I-FIT isotope predictive filtering is a strategy to reduce the number of proposed elemental compositions using algorithms to estimate the number of carbon, oxygen atoms in an unknown molecule based on the mass of the molecular ion and the relative intensity of the first two most abundant isotopes (Hobby, 2005).

All parameters used are detailed in Renard et al. (2013). Briefly, the chromatographic separations were carried out on a UPLC column (Waters, HSS T3 C18, 2.1  $\times$  100 mm – 1.8  $\mu$ m) at 40 °C. The mobile phases consisted in (A) 0.1 % formic acid (Biosolve, 99 %) in water and (B) acetonitrile (Biosolve, ULC/MS). The gradient elution was performed at a flow rate of 600  $\mu$ L min<sup>-1</sup> using 5 to 95 % of B within 7 min and held at 95 % of B for 1.5 min. The sample injection volume was 10  $\mu$ L.

During each chromatographic run, leucine enkephalin (Waters, 2 ng  $\mu$ L<sup>-1</sup>, C<sub>28</sub>H<sub>37</sub>N<sub>5</sub>O<sub>7</sub>) was used for lock-mass correction to obtain accurate masses for each organic component eluting from the column. Optimum ESI conditions were found using a 0.5 kV capillary voltage, 40 V sample cone voltage, 450 °C desolvation temperature, 120 °C source temperature, 20 L h<sup>-1</sup> cone gas flow rate and 800 L h<sup>-1</sup> desolvation gas flow rate.

All products were detected as their protonated molecules ([M + H]<sup>+</sup>) or sodium adducts ([M + Na]<sup>+</sup>) in the positive mode, and their deprotonated molecules ([M – H]<sup>-</sup>) in the negative mode. Data were collected from  $m/z$  50 to 1800 in both ionization modes.

### 2.2.2 UHPLC-UV analyses

An ultra-high-performance liquid chromatographic (UHPLC) system (ThermoScientific, Accela 600 autosampler and Accela 600 pump) coupled to a diode array detector (ThermoScientific, Accela 600 PDA detector) was used to monitor the concentrations of MVK and H<sub>2</sub>O<sub>2</sub> sampled from the photoreactor. The chromatographic separation was performed using a column (ThermoScientific, Hypersil GOLD, 100 × 2.1 mM–1.9 μm) at 40 °C and a flow rate of 300 μL min<sup>-1</sup>. The mobile phase was water/acetonitrile (98 : 2) (v/v) and the injection volume was set to 2 μL. The spectra were recorded from 200 to 360 nm.

Under these conditions, H<sub>2</sub>O<sub>2</sub> has a retention time of 0.5 min and is chromatographically separated from MVK which has a retention time of 1.8 min. The UV spectrum of aqueous H<sub>2</sub>O<sub>2</sub> exponentially increases with decreasing wavelength, and it becomes intense below 300 nm. Aqueous solutions of MVK show an intense absorption band (K-band;  $\pi \rightarrow \pi^*$  transition) that peaks at 211 nm and a weak absorption band (R-band;  $n \rightarrow \pi^*$  transition) that peaks at 308 nm. The chromatograms were monitored at 270, 229 nm and 211 nm and the peak areas were found to be directly proportional to both the H<sub>2</sub>O<sub>2</sub> and the MVK concentrations in the range of the studied concentrations: at 211 nm for low MVK concentrations ([MVK] ≤ 0.5 mM), at 229 nm for 2 ≤ [MVK] ≤ 20 mM, and at 270 nm for H<sub>2</sub>O<sub>2</sub> concentrations.

### 2.2.3 IC-ESI-MS analyses

Quantification of organic acids in the solutions was performed with an ion chromatography system (Dionex ICS3000) driven by Chromeleon<sup>®</sup> software (6.80 version), composed of a gradient pump (Dionex SP-5), an autosampler (Dionex AS40), a conductivity detector (Dionex, CD25) and coupled to a quadrupole mass spectrometer (Thermo Scientific Surveyor MSQ) operated in the negative electrospray ionization (ESI) mode, using nitrogen gas flow of 6 L h<sup>-1</sup>, 40 psi, temperature 500 °C, capillary voltage 3.5 kV, and sample cone voltage 75 V. An electrolytic suppressor (Dionex, 4 mM ASRS 300) operated in external water mode (7 mL min<sup>-1</sup>) was placed before the conductivity cell. An additional peristaltic pump was used during measurements to wash the entrance cone of the mass spectrometer with water at a flow rate of 0.4 mL min<sup>-1</sup>. The chromatographic separations were carried out on a column (Dionex, IonPac AS11-HC, 4 × 250 mM) coupled to a guard column (Dionex, AG11-HC, 4 × 50 mM). A 25 μL sample was injected automatically using a 25 μL loop injection valve. The analysis was performed at 35 °C, with a flow rate set at 0.8 mL min<sup>-1</sup>. Eluent A (ultra-high-quality water) and eluent B (100 mM NaOH) were flushed with purified helium gas for 30 min and kept under nitrogen atmosphere during the procedure. Separation was carried out using the following gradient (min, B %): 0, 1 %; 12, 5 %; 30, 19 %; 40, 40 %, 50, 1 %. The

analytes were monitored using the selected ion-monitoring (SIM) mode, and signal areas (counts min<sup>-1</sup>) of each peak were used for quantification.

### 2.2.4 TOC analyses

TOC measurements were associated with preparative liquid chromatography to separate the oligomers from the small and/or volatile reactants and reaction products in the liquid samples, in order to measure the oligomer mass yields in experiment A (see Sect. 3.2.3). A total organic carbon/total nitrogen (TOC/TN) analyzer (Analytik Jena, N/C2100S) with the non-purgeable organic carbon (NPOC) method was used to quantify the produced oligomers in our liquid samples.

The NPOC method consists in pre-purging samples with oxygen and pre-acidifying (at pH = 2 with HCl) to remove the inorganic carbon and purgeable organic carbon. TOC is measured by injecting the sample into a heated combustion tube (800 °C) with an oxidation catalyst. The CO<sub>2</sub> produced is measured by a non-dispersive infrared (NDIR) gas analyzer. TN is measured in parallel using chemiluminescence detection (CLD).

### 2.3 Particle generation and characterization

For aerosol generation, 35 mL of the solution was sampled at specific reaction times (Table 1), and nebulized using an atomizer (TSI, 3079) with a flow rate of 3.5 L min<sup>-1</sup> (Fig. 1). The generated droplet flow was led through a silica gel diffusion dryer and diluted with filtered ambient air (at 5 L min<sup>-1</sup>, using a HEPA capsule filter). A small fraction of the sample (≈ 0.4 L min<sup>-1</sup>) was passed through a Nafion dryer (Permapure, MD-110), before entering a small 100 mL glass mixing chamber and the on-line analytical devices. The obtained relative humidity was constant during all experiments at ca. 15 % measured at the entrance of the AMS (Fig. 1). The nebulization time for each sample was 30 min and, to ensure constant and reproducible aerosol generation, only the last 15 min of nebulization were employed for data analysis. To avoid memory effects, before each nebulization experiment, the system was flushed by nebulizing UHQ water for 30 min.

The number size distribution was measured using a scanning mobility particle sizer (SMPS) (Grimm, SMPS + C) consisting of a differential mobility analyzer (L-DMA) with a condensation particle counter (Grimm, CPC, 5.403). The analysed particle size ranged from 11 to 1083 nm (scanned within 6 min and 43 s).

A high-resolution time-of-flight aerosol mass spectrometer was used to measure the bulk chemical composition of the non-refractory submicron particulate matter (De Carlo et al., 2006; Canagaratna et al., 2007). The instrument was used under standard conditions (vaporizer at 600 °C and electron ionization at 70 eV), in the high-sensitivity V-mode with a resolving power of 2000 at *m/z* 200. Each measurement point was averaged for 2 min and 40 s (MS cycle and PToF cycle,

40 s each, two cycles per run). Mass spectra of filtered air, using a HEPA capsule filter, were taken prior each series of nebulizing experiments in order to adjust the  $m/z$  44 entry of the fragmentation table due to gas-phase  $\text{CO}_2$ .

The standard fragmentation table with the corrected air fragment column for our carrier gas and the default values of relative ionization efficiency were used in the AMS data analysis (Squirrel 1.51H and the software PIKA 1.10 H).

### 3 Results

#### 3.1 Evidence for oligomer formation and aging

During MVK- $\bullet\text{OH}$  oxidation, the aqueous-phase composition was monitored and compared to the composition of the corresponding nebulized solutions.

##### 3.1.1 Aqueous-phase analyses

For each experiment, the solution was directly monitored using UPLC-ESI-MS and UHPLC-UV for reaction times up to 150 min (Table 1). This time was higher than the complete consumption of MVK in order to study the formation of oligomers and their aging processes, as illustrated in Fig. 2.

During experiment B (i.e.  $[\text{MVK}]_0 = 5 \text{ mM}$ ), after 5 min of reaction, no significant formation of high molecular weight compounds was observed (Fig. 2b), whereas after 10 min of reaction, mass spectra show that oligomer systems were formed on the whole range of the investigated  $m/z$  (50–1800), with a regular pattern of 70 042 amu, which corresponds to the exact mass of MVK. At 50 min of reaction, the maximum of oligomerization was reached (Fig. 2c). At this time, we observed several series of MVK oligomers, corresponding to several initiator radicals identified by Renard et al. (2013) under similar conditions. As an example, a tentative molecular structure of the most intense series is given in Fig. 2c and is highlighted in red in the mass spectrum. At that time, 90 % of MVK was consumed. Finally, the intensities of all the oligomer series decreased simultaneously for all masses with no change in the oligomer pattern up to 90 min. From this reaction time, the mass spectra show a collapse of the regular pattern in both negative (Fig. 2d, 150 min) and positive modes, possibly corresponding to a drastic aging process in which oligomers formed smaller molecules. This hypothesis is confirmed by a more global approach, using the SMPS and the AMS analysis of the SOA formed after nebulization of the solutions.

##### 3.1.2 Aerosol composition of SOA generated after nebulization of the solutions

Under similar conditions, we verified as done in a previous study (Liu et al., 2012) that nebulization of the reacted solutions and subsequent aerosol particle drying processes induced negligible chemical transformations of the oligomers

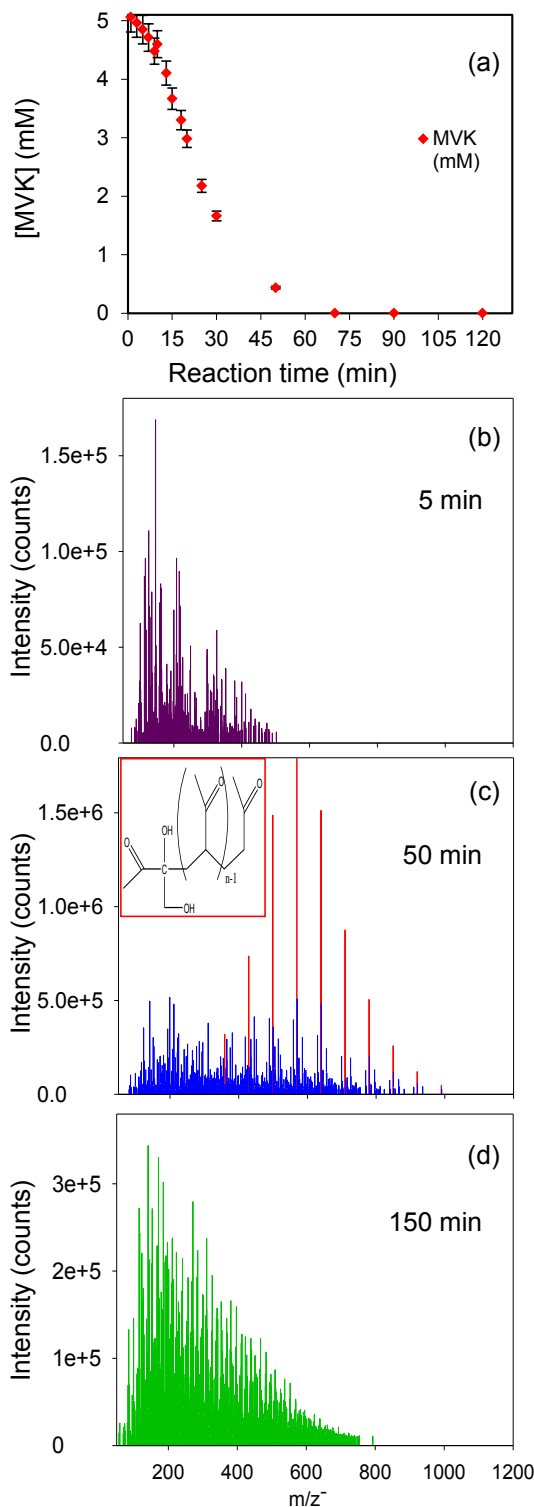


**Figure 2.** (a) Time profiles of MVK concentrations during the reaction (experiment B); and the corresponding evolution of ESI-MS spectra for  $m/z$  50–1200 at (b) 5 min, (c) 50 min and (d) 150 min. Highlighted in red in (c), the most intense peaks of the main series of oligomers together with their related molecular structure.

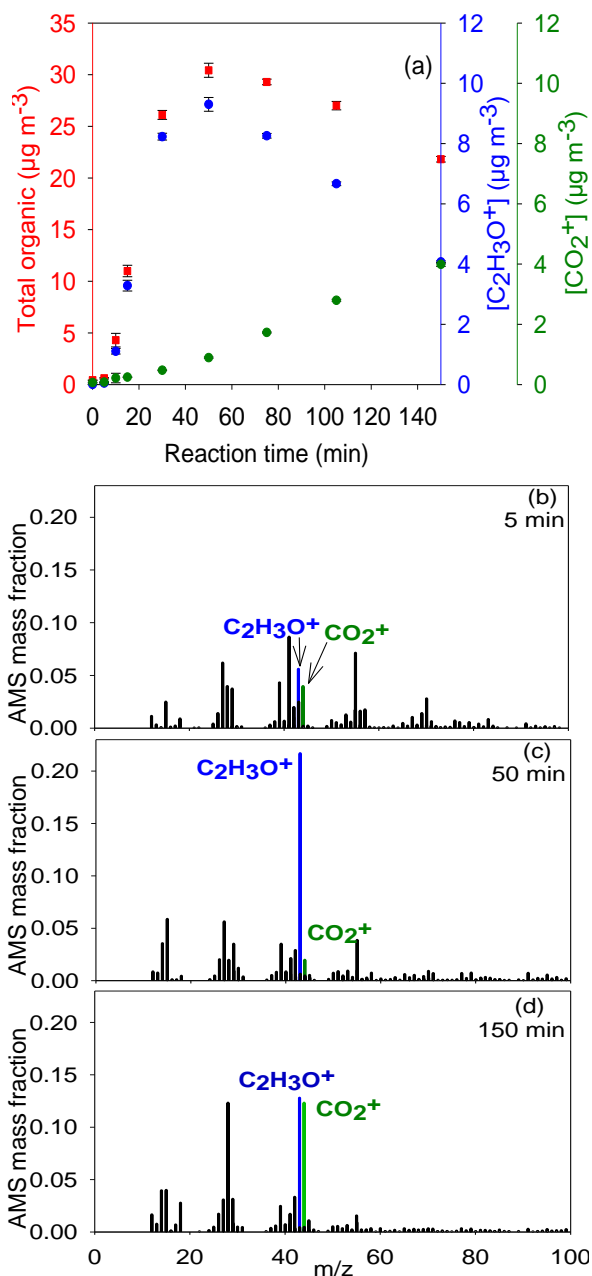


**Figure 3.** Time profiles of the HR-ToF-AMS total organic mass (red), ion fragments  $\text{C}_2\text{H}_3\text{O}^+$  at  $m/z$  43 (blue) and  $\text{CO}_2^+$   $m/z$  44 (green) for nebulized solutions from experiment B (a), and the corresponding evolution of HR-ToF-AMS mass spectra (for  $m/z$  0–100) for nebulized solutions sampled after 5 min (b), 50 min (c) and 150 min (d). Values are averages of five consecutive HR-ToF-AMS runs; error bars represent their standard deviations. The AMS mass fraction is the signal intensity contribution of each fragment to the total signal.

compared to the aqueous-phase composition. It was thus meaningful to compare the compositions of aqueous phase and SOA after nebulization.

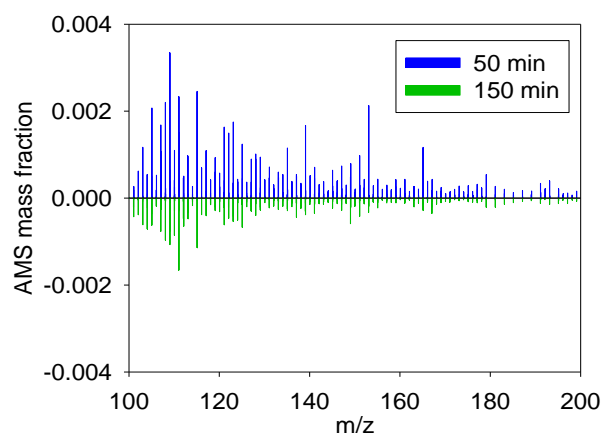


**Figure 4.** Comparison of HR-ToF-AMS mass spectra (in the range 100–200 amu) of the nebulized solutions sampled from experiment B after 50 and 150 min of reaction in the aqueous phase. The AMS mass fraction is the signal intensity contribution of each fragment to the total signal.

The AMS mass spectra (Fig. 3) show two dominant fragments, at  $m/z$  43 and  $m/z$  44, corresponding to  $\text{C}_2\text{H}_3\text{O}^+$  and  $\text{CO}_2^+$  fragments respectively. The time profiles of the AMS total organic mass and both fragments clearly show (Fig. 3) a similar kinetic behaviour as the one described above in Sect. 3.1.1 for the corresponding solutions (Fig. 2). Until 10 min of reaction, the intensity of the AMS total mass remains low (Fig. 3a) and the mass spectrum at 5 min (Fig. 3b) is not significantly different from the one obtained by nebulizing an aqueous solution containing the reactants before reaction, with  $m/z$  fragments lower than 100. Then, the total mass increases to reach a maximum at 50 min (Fig. 3c), an order of magnitude higher than at 5 min. The mass spectrum is dominated by the  $m/z$  43 fragment (Fig. 3c). This observation is likely due to fragmentation by electronic impact of oligomers containing repetitive carbonyl functions such as those identified in the aqueous phase as shown by the example of a tentative molecular structure in Fig. 2c. Finally, the intensity of both the total organic mass and that of  $m/z$  43 fragment decrease, the one of  $m/z$  44 increases, and they both dominate the AMS mass spectrum with the same intensity at the end of our investigation (150 min, Fig. 3d).

Furthermore, comparing the AMS mass spectra between 50 and 150 min at higher masses ( $m/z$  100–200) (Fig. 4), it is clear that, at 50 min of reaction, the mass spectrum contains more fragments in this range than at 150 min. It is thus likely that the oligomers are being significantly photooxidized through a fragmentation mechanism that forms smaller acidic compounds, as observed by Aljawhary et al. (2013) for different precursors, and it confirms the oligomer aging process suggested in Fig. 2. After 50 min, oligomer fragmentation prevails over oligomer formation.

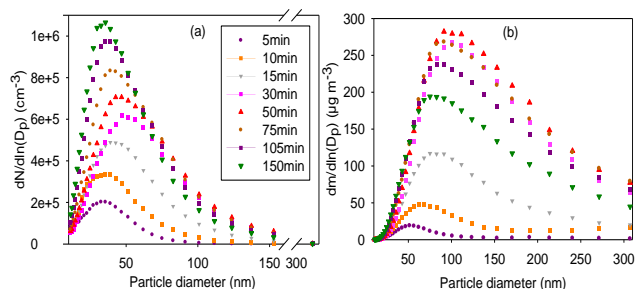


**Figure 5.** Evolution of particle number (a) and mass (b) size distributions for nebulized solutions sampled at different reaction times for experiment B, measured by means of SMPS. The standard deviations are smaller than the width of the symbols.

For the quantitative study (see Sect. 3.2), we used the data provided by the SMPS analysis. Note that the overall collection efficiencies (CEs) of the AMS in our experiments varied from 0.07 to 0.21, related to the SMPS signal. These low CE values, compared to chamber studies or ambient aerosols, can be due to particle bounce at the vaporizer surface before volatilization and to the shape- and size-dependent transmission of the aerodynamic lens. As a result, the studied compounds did not volatilize sufficiently fast at standard AMS vaporizer temperatures to be fully detected (Liu et al., 2007; Docherty et al., 2013; Miyakawa et al., 2013). In addition to these effects, it is possible that our low CE values were also due to the particle size range (50–150 nm mass distribution), as the lowest part of this size range corresponds to the region where the AMS transmission curve varies greatly (Liu et al., 2007). This effect is confirmed by the fact that our lowest values for CE (0.07) were obtained for the lowest MVK initial concentrations (0.2–2 mM) where the smallest particles were formed (50 nm mass distribution).

## 3.2 Quantitative study of SOA

### 3.2.1 SOA mass

For experiment B, Fig. 5a shows a continuously increasing number size distribution with reaction time from 5 to 150 min, with an increasing mode size during the two first kinetic steps (up to 50 min), and a decreasing mode size during the third one, which corresponds to oligomer aging. In order to determine the particle mass concentrations, we used the method described by Kuwata et al. (2012) (Eq. 1) to determine the density ( $\rho_{\text{org}}$ ) of the SOA generated in our system at each reaction time  $t$ :

$$\rho_{\text{org},t} (\text{g cm}^{-3}) = \frac{12 + 1 \times \left(\frac{\text{H}}{\text{C}}\right)_t + 16 \times \left(\frac{\text{O}}{\text{C}}\right)_t}{7.0 + 5.0 \times \left(\frac{\text{H}}{\text{C}}\right)_t + 4.15 \times \left(\frac{\text{O}}{\text{C}}\right)_t}, \quad (1)$$

where  $(\text{O}/\text{C})_t$  and  $(\text{H}/\text{C})_t$  are elemental ratios at reaction time  $t$ , as determined by the AMS analysis of the SOA

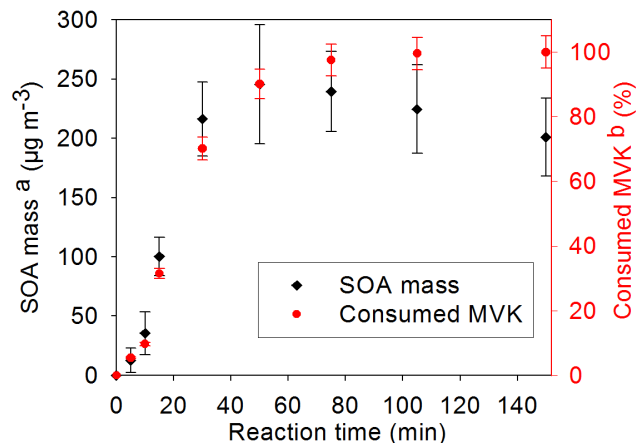


**Figure 6.** Time profiles of the total aerosol mass (black diamonds) from the nebulized solutions, and consumed MVK in the aqueous phase (red circles) for experiment B. (a) Values represent averages of three consecutive SMPS measurements for each reaction time considering the corresponding density (Table 1). Error bars represent the sum of the standard deviation of these averages and the uncertainties of the density calculation. (b) % in concentration of MVK. These concentrations were determined by means of UHPLC-UV, with an uncertainty of  $\pm 2\%$ .

formed in our system. These ratios extend to the same ranges as those used by Kuwata et al. (2012), and the resulting particle densities are reported in Table 2 and Table 3. In particular, Table 2 shows a substantial change in the H/C (decrease) and O/C (increase) after 50 min of reaction,  $t_{\text{max}}$ , for which the maximum SOA mass is reached, denoting the oligomer aging and inducing an increase of the aerosol density.

Using these particle densities, the total mass concentrations were determined, and the time evolution of the resulting distribution particle mass concentrations is shown in Fig. 5b for experiment B. The blank signal was determined prior to each individual experiment by nebulizing pure water samples and was subtracted in the results for the mass calculation. At the initial reaction time (0 min), the particle size distribution was determined by nebulizing an aqueous mixture of the reactants (using experiment B concentrations); it showed a mass concentration ( $11.0 \pm 1.4 \mu\text{g m}^{-3}$ ) not statistically different from the one obtained by nebulizing pure water, assuming a density of  $1.1 \text{ g cm}^{-3}$ . This confirms that the reactants are too volatile to form substantial amounts of organic aerosol by nebulization of the solution prior to reaction.

Confirming the UPLC-ESI-MS aqueous-phase analyses (see Sect. 3.1.1) and the AMS results (see Sect. 3.1.2), a similar kinetic behaviour is also observed on the SMPS total mass concentrations (Figs. 5b and 6). A slow increase is observed during the first step (0–10 min). Then oligomerization takes place corresponding to a fast increase of the SMPS mass, until 50 min. Finally, after this maximum of oligomerization, a significant decrease of the SMPS mass is observed. This decrease may be related to the decrease in the particle size



**Table 2.** Characteristics of the aerosol formed from nebulized MVK solutions at different reaction times for experiment B.

Reaction time (min)	$D_p$ (nm) <sup>a</sup>	$N$ ( $\times 10^3 \text{ cm}^{-3}$ ) <sup>a</sup>	H/C <sup>b</sup>	O/C <sup>b</sup>	$\rho_{\text{org}}$ ( $\text{g cm}^{-3}$ ) <sup>b, c</sup>	$M_{\text{SMPS}}$ ( $\mu\text{g m}^{-3}$ ) <sup>a, d</sup>	Yield (%) <sup>a, d, e</sup>
5	$28.3 \pm 0.7$	$90 \pm 6$	$1.55 \pm 0.02$	$0.28 \pm 0.05$	$1.0 \pm 0.2$	$10 \pm 10$	$70 \pm 80$
15	$38 \pm 1$	$530 \pm 30$	$1.55 \pm 0.01$	$0.26 \pm 0.01$	$1.1 \pm 0.1$	$100 \pm 20$	$90 \pm 60$
50	$44 \pm 1$	$860 \pm 40$	$1.55 \pm 0.01$	$0.29 \pm 0.01$	$1.1 \pm 0.1$	$240 \pm 50$	$80 \pm 50$
105	$37 \pm 1$	$1200 \pm 50$	$1.47 \pm 0.01$	$0.42 \pm 0.01$	$1.2 \pm 0.2$	$220 \pm 40$	$70 \pm 40$
150	$35 \pm 1$	$1310 \pm 50$	$1.38 \pm 0.01$	$0.57 \pm 0.01$	$1.4 \pm 0.2$	$200 \pm 30$	$60 \pm 40$

Values are the average of <sup>a</sup> three consecutive SMPS measurements, and <sup>b</sup> five consecutive O/C and H/C AMS measurements, and uncertainties represent the corresponding standard deviation of these averages.

<sup>c</sup> Particle densities are calculated using the method by Kuwata et al. (2012); the associated uncertainties include the accuracy of  $\pm 12\%$  stated by these authors for Eq. (1).

<sup>d</sup> Mass concentration values include the corresponding aerosol densities.

<sup>e</sup> Yield values and associated uncertainties include dilution + transmission efficiency determined for the nebulizing system (see Supplement 1, Table S1).

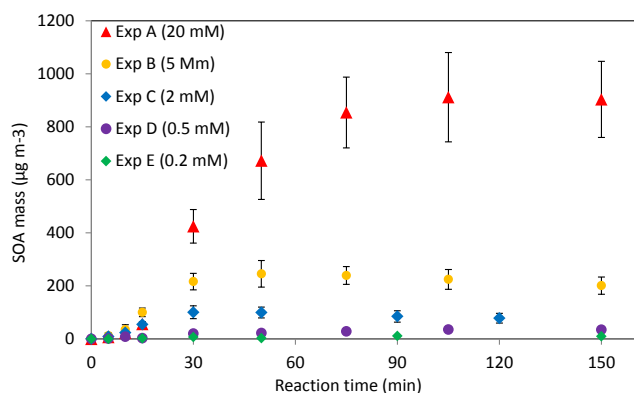


**Figure 7.** Influence of the initial MVK concentration on the evolution of the total SOA mass obtained from the nebulized solutions. Values represent averages of three consecutive SMPS measurements for each reaction time considering the corresponding density (Table 3). Error bars represent the standard deviation of these averages and the uncertainties of the density calculation. For the lowest initial concentrations (experiments D and E), blank signals were subtracted, and a density of  $1.1 \text{ g cm}^{-3}$  was assumed.

(Fig. 5a), which can be due to the decrease of the oligomer size, by fragmentation of the oligomers. It is thus likely that the oligomer aging forms more volatile compounds that the SMPS does not measure. The high correlation between the total aerosol mass concentration and the consumed MVK observed in Fig. 6 from 0 to 50 min allows for the determination of the SOA mass yield, as discussed in Sect. 3.2.3.

### 3.2.2 Influence of initial MVK concentrations

The influence of the initial aqueous-phase concentration of MVK on the SOA formation was investigated over a wide range, i.e. from 0.2 to 20 mM (Table 1). Not surprisingly, Fig. 7 shows that the total aerosol mass concentration increases with increasing initial MVK concentration. This ob-

servation is in very good agreement with the influence of MVK initial concentration on the oligomerization process observed in the aqueous phase by Renard et al. (2013). For experiments D and E, corresponding to the lowest initial MVK concentrations, the SMPS and AMS signals were low, and they could be influenced by water impurities, whereas no such influence was observed for experiments A, B and C. This is why the signal obtained from the blank experiments was subtracted only for experiments D and E in Fig. 7. Moreover, Fig. 7 clearly shows a different kinetic behaviour of the SOA mass concentration from the lowest initial concentration experiments (D and E), compared to the three highest ones (experiments A, B and C). For experiments A, B and C, the SOA mass concentration increases rapidly, reaches a maximum, and then decreases, while for experiments D and E, the signal slowly increases and does not reach a maximum. This particular evolution may be due to different chemical mechanisms occurring at different initial concentrations. We hypothesized the predominance of oligomerization at 2 mM initial concentration and above. This is further discussed in Sect. 4.

The continuous increase of the particle number (shown in Fig. 5a for experiment B) with reaction time was observed for all initial concentrations (experiments A to E), whereas the decrease of the size mode (in the number size distributions, after  $t_{\text{max}}$ ) was observed for the three highest initial concentrations only (experiments A, B and C) and not for experiments D and E, i.e. only during oligomer aging.

### 3.2.3 SOA mass yields

The SOA mass yields,  $Y_t$ , were calculated at each reaction time step  $t$  from Eq. (2):

$$Y_t = \frac{[\text{SOA}]_t}{\Delta[\text{MVK}]_t}, \quad (2)$$

where  $\Delta[\text{MVK}]_t$  is the consumed [MVK] in  $\text{mg L}^{-1}$  at reaction time  $t$ , and  $[\text{SOA}]_t$  is the formed SOA mass at reaction

**Table 3.** Overview of aerosol properties and mass yields for different initial MVK concentrations.

Exp. name	[MVK] <sub>0</sub> (mM)	<i>t</i> <sub>max</sub> (min) <sup>a</sup>	$\rho_{\text{org}}$ (g cm <sup>-3</sup> ) <sup>b</sup>	<i>M</i> <sub>SMPS</sub> (μg m <sup>-3</sup> ) <sup>b</sup>	Yield (%) <sup>b, c</sup>	H/C <sup>b</sup>	O/C <sup>b</sup>
A	20	105	1.1 ± 0.1	900 ± 200	70 ± 50	1.54 ± 0.01	0.30 ± 0.01
B	5	50	1.1 ± 0.1	240 ± 50	80 ± 50	1.55 ± 0.01	0.29 ± 0.01
C	2	30	1.1 ± 0.1	100 ± 20	80 ± 60	1.55 ± 0.01	0.28 ± 0.01

<sup>a</sup> Values are given at *t*<sub>max</sub>, corresponding to the maximum aerosol mass concentration.

<sup>b</sup> All values and associated uncertainties are calculated as indicated in Table 2.

<sup>c</sup> Including dilution + transmission efficiency (TE) in the nebulizing system; TE: 17.2 (±7.9) for [MVK]<sub>0</sub> = 2–20 mM determined from NH<sub>4</sub>NO<sub>3</sub> (see Supplement 1, Table S1).

time *t*, in mg per L of evaporated water. This term takes into account the SOA mass (*M*<sub>SMPS</sub>) measured by the SMPS at time *t* (in μg m<sup>-3</sup>), the atomizer flow (*F*<sub>atomizer</sub> in L m<sup>-3</sup>), the dilution (*f*<sub>dil</sub>), and the transmission efficiency in our nebulizing system (*T*<sub>eff</sub> in %) (see Table S1).

$$[\text{SOA}]_t = \frac{M_{\text{SMPS}} \times T_{\text{eff}}}{F_{\text{atomizer}} \times f_{\text{dil}} \times 1000} \quad (3)$$

The yields obtained at *t*<sub>max</sub> for experiments A, B and C are shown in Table 3. Although the total SOA mass (at *t*<sub>max</sub>) increases linearly with the initial concentration for these three experiments, the yields are statistically identical as well as their H/C and O/C ratios. Due to the very large uncertainties of our yield determinations (see below), it is not possible to use these data (Tables 2 and 3) to provide any interpretation on the possible effect of initial concentrations on the yields. In contrast, the O/C and H/C ratios clearly show statistically stable values when the total particle mass increases from 100 to 900 μg m<sup>-3</sup> (Table 3). It is thus likely that the total mass loading does not influence the relative oxygenation of the SOA produced (at *t*<sub>max</sub>) under our experimental conditions.

Although the particle mass loadings (*M*<sub>SMPS</sub>) were accurately measured, our yield determinations were affected by large uncertainties due to the estimation of the transmission efficiency in our nebulizing system (see Supplement 1, Table S1). In order to confirm these yields' values, another method was tested for experiment A at 90 min of reaction (i.e. close to *t*<sub>max</sub>). Preparative chromatography was performed using UPLC, where small molecules were separated from the oligomers using a divert valve, at retention times lower than 2 min. The solution containing oligomers was accumulated, concentrated and analysed using a TOC analyzer. From the carbon mass, we deduced the total mass using the H/C and O/C ratios given by the AMS. The yield was then directly calculated from the total mass of sample (in mg L<sup>-1</sup>) divided by the mass of consumed MVK at the same reaction time. A yield of 59 ± 5 % (in mass) was obtained with this method at 90 min of reaction, thus statistically similar from the one obtained by the nebulizing method (70 ± 50 %) at *t*<sub>max</sub>.

These yields are significantly higher than those obtained by Liu et al. (2012), who obtained yields up to 9.9 % under similar experimental conditions as ours. It is important to note that these values were obtained assuming all the particle densities were 1 g cm<sup>-3</sup> in Liu et al. (2012), and also the transmission efficiency of the nebulizing system was calibrated with NaCl solutions. However, it is likely that succinic acid or ammonium nitrate is more adequate for the calibration, and we show in the Supplement 1 (Table S1) that the transmission efficiencies of NaCl solutions are significantly different from the two other solutions. The nebulizing system was slightly different, with a Teflon bag in Liu et al. (2012) that could enable (i) larger amounts of wall losses for organic particles as compared to the system presented here; but (ii) longer particle residence times, leaving more time for gas–particle equilibrium than in our system. However, our control experiment using preparative chromatography confirms the high yield value obtained here, independent of the nebulizing system and its calibration. The different yields obtained here as compared to the study by Liu et al. (2012) may be due to the different irradiation Xe lamp used: 300 W, with a Pyrex filter, in Liu et al. (2012), and 1000 W, with an ASTM 490 AM 0 filter, in the present study. The influence of the lamp spectra on SOA mass yields of other systems, i.e. gas-phase photooxidation of biogenic and anthropogenic precursors, has been previously observed in atmospheric simulation chambers (Bregonzio-Rozier et al., 2014). We verified, using a spectroradiometer (SR-501, LOT-Oriel), that the spectral irradiance of the 300 W and the 1000 W Xe lamps at λ ≥ 400 nm represents respectively half and twice the solar irradiance intensity at sea level, for a 48.3° zenith angle (Supplement 2, Fig. S1). Due to the high variability of the irradiance in the atmosphere at λ ≥ 400 nm, as shown by the Tropospheric Ultraviolet and Visible Radiation Model ([http://cprm.acd.ucar.edu/Models/TUV/Interactive\\_TUV/](http://cprm.acd.ucar.edu/Models/TUV/Interactive_TUV/)), both lamps can be seen as representative of the natural irradiance in this wavelength range. However at 300 nm, the spectral irradiance of the 1000 W Xe lamp is 7 and 9 times higher than that of the direct solar irradiance (for a 48.3° zenith angle) and the 300 W Xe lamp respectively (Supplement 2, Fig. S1). This part of the spectrum is essential for photochemistry, and may induce differ-

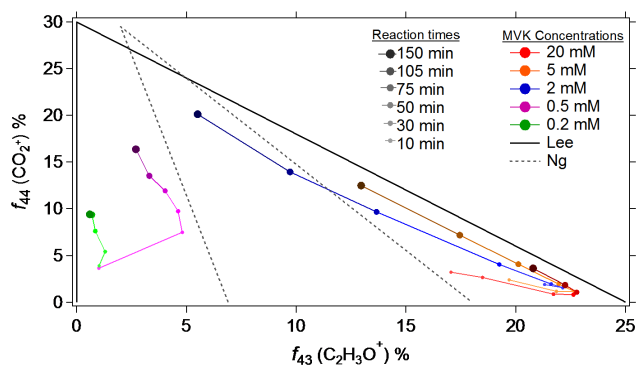


**Figure 8.** Fractions  $f_{44}$  versus  $f_{43}$  for the nebulized solutions from experiments A, B, C, D and E, as measured by the HR-ToF-AMS are compared to ambient air LV-OOA and SV-OOA from the compilation by Ng et al. (2010) (dashed black triangle), and are also compared to the nebulization data by Lee et al. (2011a) (dotted grey triangle). For our experiments, the signal from blank experiments was subtracted. The data are shown for experiments A, B, and C from 10 to 150 min of reaction, and for experiments D and E from 15 to 150 min of reaction. The gas–particle partitioning in our set-up may alter the relative oxygenation of the OA produced, especially at low initial concentrations.

ent photochemical processes: we verified that we observed the same series of oligomers as in Liu et al. (2012), but with different relative intensities. The different spectral irradiance of the lights used at 300 nm may be the reason for the different yields obtained, but it needs to be confirmed by a thorough study of the influence of the spectral irradiance in the UV, on the oligomer mass yields.

It is interesting to note that the yields and densities obtained in the present study are in the same range as those of a similar study with a different precursor, i.e. glycolaldehyde and a different irradiation system even more intense in the UV, i.e. a 254 nm mercury lamp (Ortiz-Montalvo et al., 2012). They reported aqSOA yields for oxidation products of glycolaldehyde (1 mM) which decrease gradually with reaction time from about 120 to 50 %, while the calculated densities increase from 1.3 to 1.6 g cm<sup>-3</sup>.

#### 4 Discussion

This section discusses the results obtained on the aging of the reaction products of MVK-•OH experiments and the related oxidation processes in two ways. First, the competition between functionalization and oligomerization and the subsequent aging according to the initial concentration of MVK is discussed; second, a van Krevelen diagram (i.e. H/C vs. O/C ratios) of the obtained SOA is presented and compared to previous studies.

#### 4.1 MVK functionalization versus oligomerization: influence of initial concentration

In order to compare our work with the aging of organic aerosol in the atmosphere compiled by Ng et al. (2010), we used the AMS data and, in particular, the two dominant fragments,  $m/z$  44 ( $\text{CO}_2^+$ ) and  $m/z$  43 ( $\text{C}_2\text{H}_3\text{O}^+$ ), observed in our study. More precisely, we focused on the ratio of  $m/z$  44 and  $m/z$  43 to total organic aerosol,  $f_{44}$  and  $f_{43}$ , respectively. In Ng et al. (2010), low-volatility oxygenated organic aerosol (LV-OOA) has higher  $f_{44}$  than semi-volatile oxygenated organic aerosol (SV-OOA) which in turn has higher  $f_{43}$  values. Despite the very different conditions, it is interesting to compare our aging data with those compiled from field studies and other aqueous-phase experiments. Figure 8 compares our  $f_{44}$  vs.  $f_{43}$  values to those provided in the compilation by Ng et al. (2010) as well as the nebulization data by Lee et al. (2011a). It is clear from this figure that the SOA composition and its evolution highly depend on the initial MVK concentration. For the three highest initial concentrations (experiments A, B and C), oligomerization takes place with the formation of oligomers containing repetitive carbonyl functions such as those identified in the aqueous phase (Fig. 2c), inducing an important increase of  $f_{43}$  and a simultaneous decrease of  $f_{44}$ , roughly up to  $t_{\text{max}}$ . After  $t_{\text{max}}$ , most of the initial MVK is consumed, slowing down the oligomerization process, and an important decrease of  $f_{43}$  and a simultaneous increase of  $f_{44}$  is observed, likely due to oligomer aging, as detailed in Sect. 3.1. At lower initial MVK concentrations (experiments D and E), oligomerization seems much less important and oxidation is the dominant process, as evidenced by the continuous increase of  $f_{44}$ . It can thus be suggested that, at these lower initial concentrations, functionalization dominates over oligomerization, and the aerosol is mainly composed of low-volatility organic acid and not of MVK oligomers.

This observation is strengthened by the comparison of our results with those of previous studies. Zhang et al. (2010) performed aqueous-phase •OH oxidation of MVK (0.2 mM initial concentration), and observed the formation of functionalization products, i.e. formaldehyde, glyoxal, methylglyoxal, pyruvic, oxalic, formic, acetic, and malonic acids. Furthermore, for experiments D and E ( $[\text{MVK}]_0 \leq 0.5$  mM), our  $f_{44} - f_{43}$  plots are similar to those obtained using a similar set-up, starting from pinonic acid, glyoxal and glyoxylic acid at similar and higher initial concentrations (Lee et al., 2011a, b). In particular, starting at 3 mM of glyoxal, Lee et al. (2011b) obtained similar  $f_{44} - f_{43}$  plots as our experiments performed at much lower initial concentrations ( $[\text{MVK}]_0 \leq 0.5$  mM), thus showing that the concentration is not the only important parameter in oligomerization processes, but the chemical nature of the precursor is also fundamental.

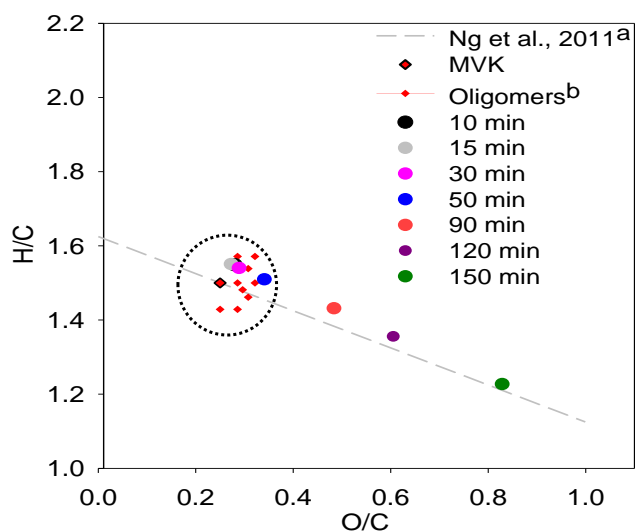


**Figure 9.** Van Krevelen diagram for the nebulized solutions of experiment C, as measured by the AMS. Only experiment C is shown for clarity as the data for experiments A and B are stacked together with the data shown. (a) Ng et al., 2011, for details see text Sect. 4.2. (b) Red diamonds represent the elemental ratios of oligomers with a degree of polymerization = 5 for the 10 most abundant oligomer series identified by Renard et al. (2013). The black dotted circle highlights compounds with similar structures.

MVK oligomerization occurs via saturation of the vinyl group (Renard et al., 2013). The resulting radical monomer is stabilized by the resonance effect with the adjacent carbonyl group, and this stabilization decreases the enthalpy of polymerization and hence facilitates the oligomerization in the aqueous phase compared to other molecules (Odian, 2004).

#### 4.2 Oligomer aging processes

The van Krevelen diagram (Fig. 9) shows a significant increase of O/C and a significant decrease of H/C with reaction time after  $t_{\max}$ . When oligomerization is the dominating process, almost no changes are observed in the van Krevelen diagram: the H/C and O/C values are confined in a restricted circle until  $t_{\max}$ . The atomic ratios for H/C and O/C of MVK and the oligomers, with a degree of polymerization of 5, identified by Renard et al. (2013) are also reported in this diagram. MVK, oligomers and the nebulized solutions until  $t_{\max}$  are confined in a circle that highlights the similarity of their structures.

After that time, the values of O/C (H/C) increase (decrease) out of the circle, thus denoting an oligomer aging process. Changes in functionality of organic aerosol are traced in this diagram along a line, whose slope is  $-0.6$ . A very similar slope value ( $-0.5$ ) was interpreted by Ng et al. (2011) as a COOH group addition to the site of a C–C bond cleavage, thus suggesting that the oligomer aging process proceeds via fragmentation. This is also suggested by the time

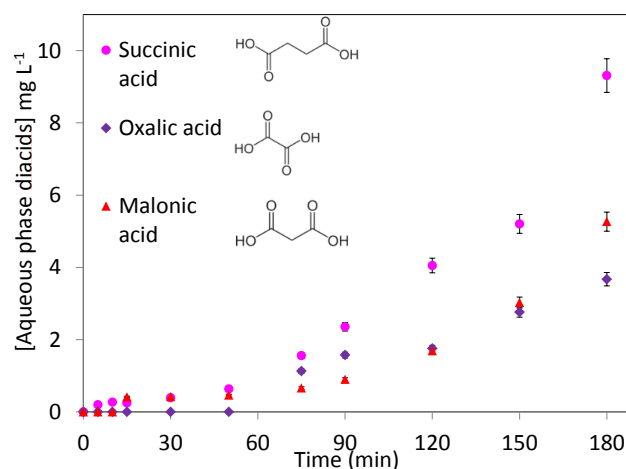


**Figure 10.** Time profiles of the quantified diacids in the solutions as measured by IC-ESI-MS for experiment B ( $[MVK]_0 = 5$  mM).

evolution of the particle number size distributions (Fig. 5a: see Sect. 3.2.1). While a continuous increase of the particle number with reaction time was observed for all initial concentrations, a significant decrease of the size mode was observed after  $t_{\max}$  for the highest concentrations only (experiments A, B and C), i.e. during oligomer aging. This size mode decrease was also correlated with a decreasing total mass (Fig. 5b). These observations, in combination with the fact that  $f_{44}$  increases during oligomer aging, indicate that the oligomer aging proceeds via fragmentation processes that generate smaller (or more volatile) and more acidic compounds.

The formation of carboxylic acids in the aqueous phase was monitored during the course of the reaction. In good agreement with Zhang et al. (2010), small volatile monocarboxylic acids such as acetic, formic and pyruvic acids were formed as primary reaction products from MVK reactivity. We further observed the formation of diacids as secondary or tertiary reaction products, such as oxalic, malonic, succinic (Fig. 10) malic and tartaric acids (not quantified). Finally, the formation of these diacids started at  $t_{\max}$ , and was correlated to the increase of the AMS  $m/z$  44 ( $\text{CO}_2^+$ ) signal observed from the nebulized solutions. It is thus likely that the oligomer aging proceeds via fragmentation (by  $\bullet\text{OH}$  oxidation and/or photolysis), leading to the formation of smaller partially oxidized products, i.e. hydroxyacids or ketoacids (such as those identified by Jaoui et al., 2006), which in turn are oxidized into stable diacids.

#### 5 Atmospheric implications

Considering the results obtained here on oligomer formation and aging from MVK at varying initial concentrations together with those obtained by previous studies on the identification of the low-molecular-weight compounds products

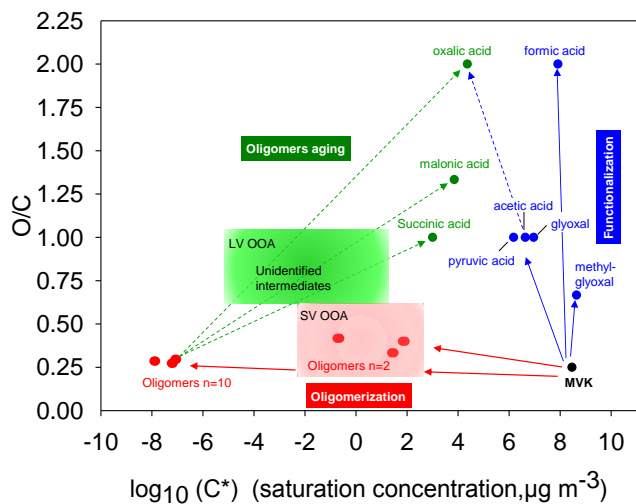


**Figure 11.** Potential atmospheric fate of MVK in the aqueous phase. The x axis denotes volatility ( $\log_{10}$  of  $C^*$  at 298K); the y axis denotes oxidation state, approximated by O/C (Jimenez et al., 2009).

of the reaction (Zhang et al., 2010), a general scheme of the potential atmospheric fate of MVK in the aqueous phase is shown on Fig. 11. MVK  $\bullet$ OH oxidation undergoes kinetic competition between functionalization and oligomerization, depending on the precursor initial concentration. At 2 mM of MVK and above this concentration, oligomerization dominates over functionalization. At these concentrations,  $\bullet$ OH oxidation of MVK forms oligomers that are SV-OOA, with low O/C (lower than 0.50) and high  $f_{43}$ . Oligomers are then fragmented, via unidentified intermediates that have the properties of LV-OOA (with increasing O/C and decreasing H/C, Fig. 9) which then form organic diacids. For lower initial MVK concentrations ( $< 2$  mM), oligomerization is not the major process, and functionalization dominates, ending into small carbonyls, dicarbonyls and acids that were identified by Zhang et al. (2010) (Fig. 11).

Among the atmospherically relevant alkenoic alcohols, acids, ketones and aldehydes, i.e. UWSOCs, although MVK is one of the most abundant species, it is one of the most volatile ( $P_{\text{sat}} = 10^{-5}$ –0.1 atm, with  $P_{\text{sat}}(\text{MVK}) = 0.1$  atm at 25 °C; Asher and Pankow 2006), and one of the least soluble compounds ( $K_{\text{H}} = 1$ – $10^3$  M atm $^{-1}$ , with  $K_{\text{H}}(\text{MVK}) = 41$  M atm $^{-1}$  at 25 °C; Iraci et al., 1999). The atmospheric impacts of the processes shown here should thus be very limited for MVK alone. However, the oligomerization mechanism undergone by MVK occurs via saturation of the vinyl group (Renard et al., 2013), and the resulting radical monomer is stabilized by the resonance effect with the adjacent carbonyl group thus decreasing the enthalpy of polymerization facilitating the oligomerization in the aqueous phase compared to other molecules. More generally, “conjugation of the  $C = C$  with substituents such as the benzene ring (styrene and  $\alpha$ -methylstyrene), and alkene double bond (butadiene and iso-

prene), the carbonyl linkage (acrylic acid, methyl acrylate, methyl methacrylate), and the nitrile group (acrylonitrile) similarly leads to stabilization of the monomer and decreases enthalpies of polymerization” (Odian, 2004). It is thus likely that a large number of atmospherically relevant molecules can follow the same process either in the bulk or at the wet aerosol interface (Kameel et al., 2013, 2014). In this context, our results suggest that this class of compounds can impact the aerosol composition, and contribute to aqSOA formation upon water evaporation. The corresponding aqSOA mass yields seem to depend on the spectral irradiance of the light used to initiate the photochemistry, but further studies are needed to confirm this point. Finally, the aging of the oligomers formed could be an explanation, at least in part, for the presence of diacids, such as oxalic, malonic and succinic acids, observed in the ambient aerosol (Legrand et al., 2007; Kawamura et al., 2010). In Part 2 of this study, the atmospheric relevance of these processes is explored by means of multiphase box model studies.

**The Supplement related to this article is available online at doi:10.5194/acp-15-21-2015-supplement.**

**Acknowledgements.** We thank the National Research Agency ANR (project CUMULUS ANR-2010-BLAN-617-01), AXA insurances, Région Rhône-Alpes (CIBLE program) and CNRS-INSU (LEFE-CHAT AtmOrbitrap project) for funding this research. We also thank Barbara Ervens (CIRES, University of Colorado, Boulder and Chemical Sciences Division, National Oceanic and Atmospheric Administration (NOAA), Boulder, CO, USA) for valuable scientific discussions on this topic; Etienne Quivet (Aix-Marseille Université, Laboratory of Chemistry of Environment) for proofreading and Assia Smaani (Aix-Marseille Université, Laboratory of Chemistry of Environment) for contributing to the experimental work on MVK  $\bullet$ OH-oxidation experiments.

Edited by: P. Renard

## References

- Aiken, A. C., DeCarlo, P. F., Kroll, J. H., Worsnop, D. R., Huffman, J. A., Docherty, K., Ulbrich, I. M., Mohr, C., Kimmel, J. R., Sueper, D., Zhang, Q., Sun, Y., Trimborn, A., Northway, M., Ziemann, P. J., Canagaratna, M. R., Onasch, T. B., Alfarra, R., Prevot, A. S. H., Dommen, J., Duplissy, J., Metzger, A., Baltensperger, U., and Jimenez, J. L.: O/C and OM/OC ratios of primary, secondary, and ambient organic aerosols with high resolution time-of-flight aerosol mass spectrometry, *Environ. Sci. Technol.*, 42, 4478–4485, doi:10.1021/es703009q, 2008.
- Aljawhary, D., Lee, A. K. Y., and Abbatt, J. P. D.: High-resolution chemical ionization mass spectrometry (ToF-CIMS): application

- to study SOA composition and processing, *Atmos. Meas. Tech.*, 6, 3211–3224, doi:10.5194/amt-6-3211-2013, 2013.
- Altieri, K. E., Carlton, A. G., Lim, H. J., Turpin, B. J., and Seitzinger, S. P.: Evidence for oligomer formation in clouds: reactions of isoprene oxidation products, *Environ. Sci. Technol.*, 40, 4956–4960, 2006.
- Altieri, K. E., Seitzinger, S. P., Carlton, A. G., Turpin, B. J., Klein, G. C., and Marshall, A. G.: Oligomers formed through in-cloud methylglyoxal reactions: chemical composition, properties, and mechanisms investigated by ultra-high resolution FT-ICR mass spectrometry, *Atmos. Environ.*, 42, 1476–1490, 2008.
- Arakaki, T., Anastasio, C., Kuroki, Y., Nakajima, H., Okada, K., Kotani, Y., Handa, D., Azechi, S., Kimura, T., Tshako, A., and Miyagi, Y.: A general scavenging rate constant for reaction of hydroxyl radical with organic carbon in atmospheric waters, *Environ. Sci. Technol.*, 47, 8196–8203, doi:10.1021/es401927b, 2013.
- Asher, W. E. and Pankow, J. F.: Vapor pressure prediction for alkenoic and aromatic organic compounds by a UNIFAC-based group contribution method, *Atmos. Environ.*, 40, 3588–3600, doi:10.1016/j.atmosenv.2005.12.004, 2006.
- Blando, J. D. and Turpin, B. J.: Secondary organic aerosol formation in cloud and fog droplets: a literature evaluation of plausibility, *Atmos. Environ.*, 34, 1623–1632, doi:10.1016/S1352-2310(99)00392-1, 2000.
- Brégonzio-Rozier, L., Siekmann, F., Giorio, C., Pangui, E., Morales, S. B., Temime-Roussel, B., Gratien, A., Michoud, V., Ravier, S., Tapparò, A., Monod, A., and Doussin, J.-F.: Gaseous products and Secondary Organic Aerosol formation during long term oxidation of isoprene and methacrolein, *Atmos. Chem. Phys. Discuss.*, 14, 22507–22545, doi:10.5194/acpd-14-22507-2014, 2014.
- Canagaratna, M. R., Jayne, J. T., Jimenez, J. L., Allan, J. D., Alfarra, M. R., Zhang, Q., Onasch, T. B., Drewnick, F., Coe, H., Middlebrook, A., Delia, A., Williams, L. R., Trimborn, A. M., Northway, M. J., DeCarlo, P. F., Kolb, C. E., Davidovits, P., and Worsnop, D. R.: Chemical and microphysical characterization of ambient aerosols with the aerodyne aerosol mass spectrometer, *Mass Spectrom. Rev.*, 26, 185–222, 2007.
- Carlton, A. G. and Turpin, B. J.: Particle partitioning potential of organic compounds is highest in the Eastern US and driven by anthropogenic water, *Atmos. Chem. Phys.*, 13, 10203–10214, doi:10.5194/acp-13-10203-2013, 2013.
- Carlton, A. G., Turpin, B. J., Altieri, K. E., Seitzinger, S., Reff, A., Lim, H. J., and Ervens, B.: Atmospheric oxalic acid and SOA production from glyoxal: results of aqueous photooxidation experiments, *Atmos. Environ.*, 41, 7588–7602, doi:10.1016/j.atmosenv.2007.05.035, 2007.
- Carlton, A. G., Turpin, B. J., Lim, H.-J., Altieri, K. E. and Seitzinger, S.: Link between isoprene and secondary organic aerosol (SOA): Pyruvic acid oxidation yields low volatility organic acids in clouds, *Geophys. Res. Lett.*, 33(6), doi:10.1029/2005GL025374, 2006.
- Carlton, A. G., Wiedinmyer, C., and Kroll, J. H.: A review of Secondary Organic Aerosol (SOA) formation from isoprene, *Atmos. Chem. Phys.*, 9, 4987–5005, doi:10.5194/acp-9-4987-2009, 2009.
- Daumit, K. E., Carrasquillo, A. J., Hunter, J. F., and Kroll, J. H.: Laboratory studies of the aqueous-phase oxidation of polyols: submicron particles vs. bulk aqueous solution, *Atmos. Chem. Phys.*, 14, 10773–10784, doi:10.5194/acp-14-10773-2014, 2014.
- DeCarlo, P. F., Dunlea, E. J., Kimmel, J. R., Aiken, A. C., Sueper, D., Crouse, J., Wennberg, P. O., Emmons, L., Shinzuka, Y., Clarke, A., Zhou, J., Tomlinson, J., Collins, D. R., Knapp, D., Weinheimer, A. J., Montzka, D. D., Campos, T., and Jimenez, J. L.: Fast airborne aerosol size and chemistry measurements above Mexico City and Central Mexico during the MILAGRO campaign, *Atmos. Chem. Phys.*, 8, 4027–4048, doi:10.5194/acp-8-4027-2008, 2008.
- DeCarlo, P. F., Kimmel, J. R., Trimborn, A., and Northway, M. J.: Field-deployable, high-resolution, time-of-flight aerosol mass spectrometer, *Anal. Chem.*, 78, 8281–8289, 2006.
- Docherty, K. S., Jaoui, M., Corse, E., Jimenez, J. L., Offenberg, J. H., Lewandowski, M., and Kleindienst, T. E.: Collection efficiency of the aerosol mass spectrometer for chamber-generated secondary organic aerosols, *Aerosol Sci. Tech.*, 47, 294–309, 2013.
- Donahue, N. M., Epstein, S. A., Pandis, S. N., and Robinson, A. L.: A two-dimensional volatility basis set: 1. organic-aerosol mixing thermodynamics, *Atmos. Chem. Phys.*, 11, 3303–3318, doi:10.5194/acp-11-3303-2011, 2011.
- El Haddad, I., Yao Liu, Nieto-Gligorovski, L., Michaud, V., Temime-Roussel, B., Quivet, E., Marchand, N., Sellegri, K., and Monod, A.: In-cloud processes of methacrolein under simulated conditions – Part 2: Formation of secondary organic aerosol, *Atmos. Chem. Phys.*, 9, 5107–5117, doi:10.5194/acp-9-5107-2009, 2009.
- Epstein, S. A., Tapavicza, E., Furche, F., and Nizkorodov, S. A.: Direct photolysis of carbonyl compounds dissolved in cloud and fog droplets, *Atmos. Chem. Phys.*, 13, 9461–9477, doi:10.5194/acp-13-9461-2013, 2013.
- Ervens, B., Turpin, B. J., and Weber, R. J.: Secondary organic aerosol formation in cloud droplets and aqueous particles (aqSOA): a review of laboratory, field and model studies, *Atmos. Chem. Phys.*, 11, 11069–11102, doi:10.5194/acp-11-11069-2011, 2011.
- Ervens, B. and Volkamer, R.: Glyoxal processing by aerosol multiphase chemistry: towards a kinetic modeling framework of secondary organic aerosol formation in aqueous particles, *Atmos. Chem. Phys.*, 10(17), 8219–8244, doi:10.5194/acp-10-8219-2010, 2010.
- Guenther, A., Karl, T., Harley, P., Wiedinmyer, C., Palmer, P. I., and Geron, C.: Estimates of global terrestrial isoprene emissions using MEGAN (Model of Emissions of Gases and Aerosols from Nature), *Atmos. Chem. Phys.*, 6, 3181–3210, doi:10.5194/acp-6-3181-2006, 2006.
- Hallquist, M., Wenger, J. C., Baltensperger, U., Rudich, Y., Simpson, D., Claeys, M., Dommen, J., Donahue, N. M., George, C., Goldstein, A. H., Hamilton, J. F., Herrmann, H., Hoffmann, T., Iinuma, Y., Jang, M., Jenkin, M. E., Jimenez, J. L., Kiendler-Scharr, A., Maenhaut, W., McFiggans, G., Mentel, Th. F., Monod, A., Prévôt, A. S. H., Seinfeld, J. H., Surratt, J. D., Szmigielski, R., and Wildt, J.: The formation, properties and impact of secondary organic aerosol: current and emerging issues, *Atmos. Chem. Phys.*, 9, 5155–5236, doi:10.5194/acp-9-5155-2009, 2009.
- Herrmann, H., Hoffmann, D., Schaefer, T., Brüner, P., and Tilgner, A.: Tropospheric aqueous phase free radical chemistry:

- radical sources, spectra, reaction kinetics and prediction tools, *Chemphyschem*, 11, 3796–3822, 2010.
- Hobby, K.: A novel method of isotope prediction applied to elemental composition analysis, 2005.
- Iraci, L. T., Baker, B. M., Tyndall, G. S., and Orlando, J. J.: Measurements of the Henry's law coefficients of 2-methyl-3-buten-2-ol, methacrolein, and methylvinyl ketone, *J. Atmos. Chem.*, 33, 321–330, 1999.
- Jaoui, M., Corse, E., Kleindienst, T. E., Offenberg, J. H., Lewandowski, M., and Edney, E. O.: Analysis of Secondary Organic Aerosol Compounds from the Photooxidation of d-Limonene in the Presence of NO<sub>x</sub> and their Detection in Ambient PM<sub>2.5</sub>, *Environ. Sci. Tech.*, 40, 3819–3828, doi:10.1021/es052566z, 2006.
- Jimenez, J. L., Canagaratna, M. R., Donahue, N. M., Prevot, A. S. H., Zhang, Q., Kroll, J. H., DeCarlo, P. F., Allan, J. D., Coe, H., Ng, N. L., Aiken, A. C., Docherty, K. S., Ulbrich, I. M., Grieshop, A. P., Robinson, A. L., Duplissy, J., Smith, J. D., Wilson, K. R., Lanz, V. A., Hueglin, C., Sun, Y. L., Tian, J., Laaksonen, A., Raatikainen, T., Rautiainen, J., Vaattovaara, P., Ehn, M., Kulmala, M., Tomlinson, J. M., Collins, D. R., Cubison, M. J., E., Dunlea, J., Huffman, J. A., Onasch, T. B., Alfarra, M. R., Williams, P. I., Bower, K., Kondo, Y., Schneider, J., Drewnick, F., Borrmann, S., Weimer, S., Demerjian, K., Salcedo, D., Cottrell, L., Griffin, R., Takami, A., Miyoshi, T., Hatakeyama, S., Shimono, A., Sun, J. Y., Zhang, Y. M., Dzepina, K., Kimmel, J. R., Sueper, D., Jayne, J. T., Herndon, S. C., Trimborn, A. M., Williams, L. R., Wood, E. C., Middlebrook, A. M., Kolb, C. E., Baltensperger, U., and Worsnop, D. R.: Evolution of Organic Aerosols in the Atmosphere, *Science*, 326, 1525–1529, doi:10.1126/science.1180353, 2009.
- Kameel, F. R., Hoffmann, M. R., and Colussi, A. J.: OH Radical-Initiated Chemistry of Isoprene in Aqueous Media. Atmospheric Implications, *J. Phys. Chem. A*, 117, 5117–5123, doi:10.1021/jp4026267, 2013.
- Kameel, F. R., Riboni, F., Hoffmann, M. R., Enami, S., and Colussi, A. J.: Fenton Oxidation of Gaseous Isoprene on Aqueous Surfaces, *J. Phys. Chem. C*, 140725063829009, doi:10.1021/jp505010e, 2014.
- Kanakidou, M., Seinfeld, J. H., Pandis, S. N., Barnes, I., Dentener, F. J., Facchini, M. C., Van Dingenen, R., Ervens, B., Nenes, A., Nielsen, C. J., Swietlicki, E., Putaud, J. P., Balkanski, Y., Fuzzi, S., Horth, J., Moortgat, G. K., Winterhalter, R., Myhre, C. E. L., Tsigaridis, K., Vignati, E., Stephanou, E. G., and Wilson, J.: Organic aerosol and global climate modelling: a review, *Atmos. Chem. Phys.*, 5, 1053–1123, doi:10.5194/acp-5-1053-2005, 2005.
- Kawamura, K., Kasukabe, H., and Barrie, L. A.: Secondary formation of water-soluble organic acids and  $\alpha$ -dicarbonyls and their contributions to total carbon and water-soluble organic carbon: Photochemical aging of organic aerosols in the Arctic spring, *J. Geophys. Res.*, 115, doi:10.1029/2010JD014299, 2010.
- Kroll, J. H., Ng, N. L., Murphy, S. M., Flagan, R. C., and Seinfeld, J. H.: Secondary Organic Aerosol Formation from Isoprene Photooxidation, *Environ. Sci. Tech.*, 40, 1869–1877, doi:10.1021/es0524301, 2006.
- Kroll, J. H. and Seinfeld, J. H.: Chemistry of secondary organic aerosol: Formation and evolution of low-volatility organics in the atmosphere, *Atmos. Environ.*, 42, 3593–3624, doi:10.1016/j.atmosenv.2008.01.003, 2008.
- Kuwata, M., Zorn, S. R. and Martin, S. T.: Using Elemental Ratios to Predict the Density of Organic Material Composed of Carbon, Hydrogen, and Oxygen, *Environ. Sci. Technol.*, 46, 787–794, doi:10.1021/es202525q, 2012.
- Lee, A. K. Y., Hayden, K. L., Herckes, P., Leaitch, W. R., Ligio, J., Macdonald, A. M., and Abbatt, J. P. D.: Characterization of aerosol and cloud water at a mountain site during WACS 2010: secondary organic aerosol formation through oxidative cloud processing, *Atmos. Chem. Phys.*, 12, 7103–7116, doi:10.5194/acp-12-7103-2012, 2012.
- Lee, A. K. Y., Herckes, P., Leaitch, W. R., Macdonald, A. M., and Abbatt, J. P. D.: Aqueous OH oxidation of ambient organic aerosol and cloud water organics: Formation of highly oxidized products: aqueous oxidation of ambient organics, *Geophys. Res. Lett.*, 38, n/a–n/a, doi:10.1029/2011GL047439, 2011a.
- Lee, A. K. Y., Zhao, R., Gao, S. S., and Abbatt, J. P. D.: Aqueous-Phase OH Oxidation of Glyoxal: Application of a Novel Analytical Approach Employing Aerosol Mass Spectrometry and Complementary Off-Line Techniques, *J. Phys. Chem. A*, 115, 10517–10526, doi:10.1021/jp204099g, 2011b.
- Lee, W., Baasandorj, M., Stevens, P. S., and Hites, R. A.: Monitoring OH-initiated oxidation kinetics of isoprene and its products using online mass spectrometry, *Environ. Sci. Tech.*, 39, 1030–1036, 2005.
- Legrand, M., Preunkert, S., Oliveira, T., Pio, C. A., Hammer, S., Gelencsér, A., Kasper-Giebl, A., and Laj, P.: Origin of C<sub>2</sub>–C<sub>5</sub> dicarboxylic acids in the European atmosphere inferred from year-round aerosol study conducted at a west-east transect, *J. Geophys. Res.*, 112, D23S07, doi:10.1029/2006JD008019, 2007.
- Lim, Y. B., Tan, Y., and Turpin, B. J.: Chemical insights, explicit chemistry, and yields of secondary organic aerosol from OH radical oxidation of methylglyoxal and glyoxal in the aqueous phase, *Atmos. Chem. Phys.*, 13, 8651–8667, doi:10.5194/acp-13-8651-2013, 2013.
- Liu, P. S. K., Deng, R., Smith, K. A., Williams, L. R., Jayne, J. T., Canagaratna, M. R., Moore, K., Onasch, T. B., Worsnop, D. R., and Deshler, T.: Transmission Efficiency of an Aerodynamic Focusing Lens System: Comparison of Model Calculations and Laboratory Measurements for the Aerodyne Aerosol Mass Spectrometer, *Aerosol Sci. Technol.*, 41, 721–733, doi:10.1080/02786820701422278, 2007.
- Liu, Y., Siekmann, F., Renard, P., El Zein, A., Salque, G., El Haddad, I., Temime-Roussel, B., Voisin, D., Thissen, R., and Monod, A.: Oligomer and SOA formation through aqueous phase photooxidation of methacrolein and methyl vinyl ketone, *Atmos. Environ.*, 49, 123–129, doi:10.1016/j.atmosenv.2011.12.012, 2012.
- Miyakawa, T., Matsuzawa, R., Katayama, M., and Takegawa, N.: Reconsidering Adhesion and Bounce of Submicron Particles Upon High-Velocity Impact, *Aerosol Sci. Technol.*, 47, 472–481, doi:10.1080/02786826.2013.763895, 2013.
- Ng, N. L., Canagaratna, M. R., Jimenez, J. L., Chhabra, P. S., Seinfeld, J. H. and Worsnop, D. R.: Changes in organic aerosol composition with aging inferred from aerosol mass spectra, *Atmos. Chem. Phys.*, 11, 6465–6474, doi:10.5194/acp-11-6465-2011, 2011.
- Ng, N. L., Canagaratna, M. R., Zhang, Q., Jimenez, J. L., Tian, J., Ulbrich, I. M., Kroll, J. H., Docherty, K. S., Chhabra, P.

- S., Bahreini, R., Murphy, S. M., Seinfeld, J. H., Hildebrandt, L., Donahue, N. M., DeCarlo, P. F., Lanz, V. A., Prévôt, A. S. H., Dinar, E., Rudich, Y., and Worsnop, D. R.: Organic aerosol components observed in Northern Hemispheric datasets from Aerosol Mass Spectrometry, *Atmos. Chem. Phys.*, 10, 4625–4641, doi:10.5194/acp-10-4625-2010, 2010.
- Odian, G. G.: Principles of polymerization, Wiley, edited by: Hoboken, N. J., <http://public.eblib.com/EBLPublic/PublicView.do?ptiID=469767>. last access: 10 October 2014, 2004.
- Ortiz-Montalvo, D. L., Lim, Y. B., Perri, M. J., Seitzinger, S. P., and Turpin, B. J.: Volatility and Yield of Glycolaldehyde SOA Formed through Aqueous Photochemistry and Droplet Evaporation, *Aeros. Sci. Technol.*, 46, 1002–1014, doi:10.1080/02786826.2012.686676, 2012.
- Perri, M. J., Seitzinger, S., and Turpin, B. J.: Secondary organic aerosol production from aqueous photooxidation of glycolaldehyde: Laboratory experiments, *Atmos. Environ.*, 43, 1487–1497, doi:10.1016/j.atmosenv.2008.11.037, 2009.
- Renard, P., Reed Harris, A. E., Rapf, R. J., Ravier, S., Demelas, C., Coulomb, B., Quivet, E., Vaida, V., and Monod, A.: Aqueous Phase Oligomerization of Methyl Vinyl Ketone by Atmospheric Radical Reactions, *J. Phys. Chem. C*, 118, 29421–29430, 2014.
- Renard, P., Siekmann, F., Gandolfo, A., Socorro, J., Salque, G., Ravier, S., Quivet, E., Clément, J.-L., Traikia, M., Delort, A.-M., Voisin, D., Vuitton, V., Thissen, R. and Monod, A.: Radical mechanisms of methyl vinyl ketone oligomerization through aqueous phase OH-oxidation: on the paradoxical role of dissolved molecular oxygen, *Atmos. Chem. Phys.*, 13, 6473–6491, doi:10.5194/acp-13-6473-2013, 2013.
- Spracklen, D. V., Jimenez, J. L., Carslaw, K. S., Worsnop, D. R., Evans, M. J., Mann, G. W., Zhang, Q., Canagaratna, M. R., Allan, J., Coe, H., McFiggans, G., Rap, A., and Forster, P.: Aerosol mass spectrometer constraint on the global secondary organic aerosol budget, *Atmos. Chem. Phys.*, 11, 12109–12136, doi:10.5194/acp-11-12109-2011, 2011.
- Surratt, J. D., Murphy, S. M., Kroll, J. H., Ng, N. L., Hildebrandt, L., Sorooshian, A., Szmigielski, R., Vermeylen, R., Maenhaut, W., Claeys, M., Flagan, R. C., and Seinfeld, J. H.: Chemical Composition of Secondary Organic Aerosol Formed from the Photooxidation of Isoprene, *J. Phys. Chem. A*, 110, 9665–9690, doi:10.1021/jp061734m, 2006.
- Tan, Y., Carlton, A. G., Seitzinger, S. P., and Turpin, B. J.: SOA from methylglyoxal in clouds and wet aerosols: Measurement and prediction of key products, *Atmos. Environ.*, 44, 5218–5226, doi:10.1016/j.atmosenv.2010.08.045, 2010.
- Tan, Y., Lim, Y. B., Altieri, K. E., Seitzinger, S. P., and Turpin, B. J.: Mechanisms leading to oligomers and SOA through aqueous photooxidation: insights from OH radical oxidation of acetic acid and methylglyoxal, *Atmos. Chem. Phys.*, 12, 801–813, doi:10.5194/acp-12-801-2012, 2012.
- Tan, Y., Perri, M. J., Seitzinger, S. P., and Turpin, B. J.: Effects of Precursor Concentration and Acidic Sulfate in Aqueous Glyoxal–OH Radical Oxidation and Implications for Secondary Organic Aerosol, *Environ. Sci. Technol.*, 43, 8105–8112, doi:10.1021/es901742f, 2009.
- Volkamer, R., San Martini, F., Molina, L. T., Salcedo, D., Jimenez, J. L. and Molina, M. J.: A missing sink for gas-phase glyoxal in Mexico City: Formation of secondary organic aerosol, *Geophys. Res. Lett.*, 34, doi:10.1029/2007GL030752, 2007.
- Zhang, X., Chen, Z. M., and Zhao, Y.: Laboratory simulation for the aqueous OH-oxidation of methyl vinyl ketone and methacrolein: significance to the in-cloud SOA production, *Atmos. Chem. Phys.*, 10, 9551–9561, doi:10.5194/acp-10-9551-2010, 2010.
- Zhao, R., Lee, A. K. Y., and Abbatt, J. P. D.: Investigation of Aqueous-Phase Photooxidation of Glyoxal and Methylglyoxal by Aerosol Chemical Ionization Mass Spectrometry: Observation of Hydroxyhydroperoxide Formation, *J. Phys. Chem. A*, 116, 6253–6263, doi:10.1021/jp211528d, 2012.